

Analytical and Experimental Characterization of Flow in Slowly-Varying Cross-section Microchannels

M. Akbari

Mechatronic System Engineering School of
Engineering Science, Simon Fraser University,
Surrey, BC, V3T 0A3, Canada.

M. Bahrami

Mechatronic System Engineering School of
Engineering Science, Simon Fraser University,
Surrey, BC, V3T 0A3, Canada.

D. Sinton

Department of Mechanical Engineering,
University of Victoria, Victoria, BC, V8W 2Y2,
Canada.

ABSTRACT

This paper outlines a novel approximate solution for determining the pressure drop of laminar, single-phase flow in slowly-varying microchannels of arbitrary cross-section. The proposed analysis is general and applicable to symmetric and asymmetric microchannel cross-sections, as examples compact relationships are reported for elliptical and rectangular shapes for three common wall profiles of linear, sinusoidal and hyperbolic. An experimental setup is designed and pressure drop measurements are conducted to validate the proposed model for streamwise periodic microchannels with rectangular cross-section and linear wall with a range of channel geometrical parameters such as aspect ratio and channel slope. The model is also compared against the numerical and experimental data of hyperbolic contraction with rectangular cross-section collected by others. It is observed that although the proposed model is based on the solution of the elliptical cross-section, it can accurately predict the pressure drop in microchannels of rectangular cross-section.

NOMENCLATURE

| | | |
|---------|---|--|
| A | = | Cross-sectional area, m^2 |
| a | = | Ellipse major axis/rectangle width, m |
| a_c | = | Minimum width of the hyperbolic contraction, m |
| a_u | = | Maximum width of the hyperbolic contraction, m |
| b | = | Ellipse minor axis/rectangle height, m |
| I_p | = | Polar momentum of cross-sectional area, m^4 |
| I_p^* | = | Dimensionless polar momentum of inertia, - |
| Re | = | Reynolds number, $\rho U_0 \sqrt{A} / \mu$ |

| | | |
|---------------|---|---|
| R_f | = | Flow resistance, $\Delta p / Q$ |
| $R_{f,0}$ | = | Flow resistance of a reference straight channel, $pa \cdot s / m^3$ |
| U_0 | = | Reference average velocity, Q / A_0 |
| GREEK | | |
| ε | = | Perturbation parameter, $\sqrt{A_0} / \lambda$ |
| λ | = | Channel length, m |
| ξ | = | Deviation parameter, δ / a_0 |

1. INTRODUCTION

Recently, a noticeable trend in the use of microfluidic and lab-on-chip devices; applications include analysis of DNA and proteins [1], sorting of cells [2,3], high-throughput screening [4], chemical reactions [5], and transfer of small volumes (1 to 100 nL) of materials [6]; motivated new research questions in fluid dynamic at small scales. Particularly active research areas are micromixer design [7-17], accelerated particle electrophoresis [18, 19], heat transfer augmentation in micro heat sinks [20-22], flow through porous media [23-26], blood flow in the context of biomechanics [27], temperature gradient focusing [28, 29] in analytical chemistry, and polymer processing [30, 31].

There are several studies in the literature that focused on finding the pressure drop and velocity distribution in channels with varying cross-section. The previous investigations can be divided into three categories: (i) analytical methods [32-38]; (ii) numerical methods [20, 39, 40]; and (iii) experimental studies [30,31, 41, 42]. The available solutions give velocity distribution in an axisymmetric geometries (i.e. circular cross-section) or parallel wavy plate.

Various solutions exist for low Reynolds number flow of a Newtonian fluid through axisymmetric constricted tubes or two dimensional symmetric constricted channels [32-38]. A simple model is to approximate the flow by assuming that the fluid

flow resembles the fully developed flow at each axial location along the channel; this is usually referred to as the “lubrication approximation” [43]. The overall pressure drop is then calculated by integrating the locally Poiseuille equation over the length of the channel. Although good results can be obtained for creeping flow in mildly constricted channels, this method is not very accurate when the inertia effects become important or the amplitude of the constriction is substantial. In order to bypass the full analysis of this problem, “asymptotic series solution” is used by many authors for sinusoidal tubes [32, 36], two-dimensional channels with sinusoidal walls [35], and elliptical cross-section channels [34]. In this method, the solution of the Navier-Stokes equations is obtained by expanding the flow variables in powers of a small parameter characterizing the slowly varying character of the bounding walls; usually referred to as “perturbation parameter”. Although the asymptotic solution method gives more accurate results compared to the lubrication approximation, finding a solution for flows in arbitrary three-dimensional channels is highly unlikely. Numerical methods are usually used for different channels cross-sections [31, 39, and 40] which gives good agreement with experimental data even beyond the critical Reynolds number for the onset of flow recirculation. However, the drawback is that much computational time is required, which is not suitable when a large number of channels are being investigated.

As a result of recent advances in microfabrication techniques, microchannels with different cross sectional geometries are fabricated for both commercial and scientific purposes. Finding analytical solutions for many practical cross-sections, such as rectangular or trapezoidal microchannels, is complex and/or impossible. In many engineering applications such as basic design and optimization, it is often required to obtain the trends and a reasonable estimate of the pressure drop. Bahrami et al. [45] developed a general model for prediction of pressure drop in microchannels of arbitrary cross section. Using the analytical solution of elliptical duct and the concept of Saint-Venant principle in torsion [46], they showed that the Poiseuille number, $f Re$ [45], is a function of the polar moment of inertia, area, and perimeter of the cross section of the channel. Their model showed good agreement with experimental and numerical data for a wide variety of cross sections such as rectangular, trapezoidal, triangular, circular, and moon shaped. The model of Bahrami et al., however, is restricted to straight channels. As a result, the major focus of this paper is to extend the model of Bahrami et al. [45] to the slowly-varying microchannels of arbitrary cross-sections and propose an accurate approximate method that can predict the pressure drop for slowly-varying microchannels of arbitrary cross-section. Another purpose of this work is to present compact solutions that can predict the pressure loss along the slowly varying microchannels of various cross-sections for very low and moderate Reynolds numbers.

This paper is organized as follows: Sec. 2 is dedicated to the problem statement and governing equations. In Sec. 3, under the assumption of slowly varying cross-section, a general

approach for determining the pressure drop in microchannels of arbitrary cross-section is proposed; lubrication approximation and inertia effects are also discussed. The present method is applicable to all channel types; as examples in Sec. 4 compact models are reported for elliptical and rectangular cross-sections for three common wall shapes. In Sec.5, sample preparation, experimental setup, and test procedure are explained. The comparison between experimental data and the present model along with the results and discussion are presented in Sec. 6. Section 7 is the summary and conclusion.

2.PROBLEM STATEMENT

Figure 1 schematically shows a slowly-varying microchannel of arbitrary cross-section with the length of λ , where the Reynolds number is low to moderate. The equations of motion and mass conservation for steady-state flow of a Newtonian fluid with constant properties in Cartesian coordinates $(\lambda x, Ly, Lz)$ are

$$\nabla \cdot \mathbf{u} = 0 \quad (1)$$

$$Re\varepsilon(\mathbf{u} \cdot \nabla)\mathbf{u} = -\frac{\partial p}{\partial x} + \left[\varepsilon^2 \frac{\partial^2 u}{\partial x^2} + \frac{\partial^2 u}{\partial y^2} + \frac{\partial^2 u}{\partial z^2} \right] \quad (2)$$

$$Re\varepsilon^3(\mathbf{u} \cdot \nabla)v = -\frac{\partial p}{\partial y} + \varepsilon^2 \left[\varepsilon^2 \frac{\partial^2 v}{\partial x^2} + \frac{\partial^2 v}{\partial y^2} + \frac{\partial^2 v}{\partial z^2} \right] \quad (3)$$

$$Re\varepsilon^3(\mathbf{u} \cdot \nabla)w = -\frac{\partial p}{\partial z} + \varepsilon^2 \left[\varepsilon^2 \frac{\partial^2 w}{\partial x^2} + \frac{\partial^2 w}{\partial y^2} + \frac{\partial^2 w}{\partial z^2} \right] \quad (4)$$

with no-slip boundary condition on the channel wall. In Eqs. (1)-(4), L is a characteristic length scale, $\varepsilon = L/\lambda$ is the perturbation parameter, $Re = U_0 L/\nu$ is the Reynolds number and U_0 is a scale for the axial velocity component. The velocity field \mathbf{u} is scaled such that each dimensionless component is $O(1)$ and is taken to be

$$\hat{\mathbf{u}} = U_0(\mathbf{u}, \varepsilon v, \varepsilon w) \quad (5)$$

and pressure is nondimensionalized as follows

$$\hat{p} = \left(\frac{\rho U_0^2}{\varepsilon Re} \right) p \quad (6)$$

The solution to in Eqs (1)-(4) is in the form a power series of ε , on the assumption that $\varepsilon \ll 1$

$$\mathbf{u} = \sum_0^{\infty} \varepsilon^i \mathbf{u}_i \quad (7)$$

Using a similar expression for pressure, p , substituting into the governing equations, Eqs. (1)-(4), and applying the boundary conditions, u_i and p_i can be determined. The above

mentioned procedure is general and does not depend on the geometry of the microchannel.

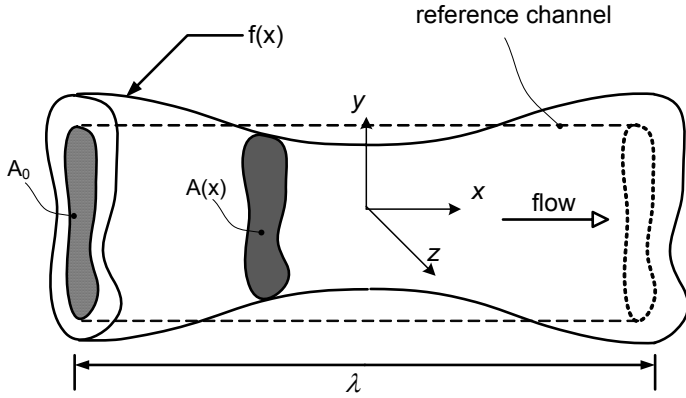


Figure 1. Schematic of a slowly varying microchannel with arbitrary wall shape of $f(x)$. A_0 is the cross-sectional area of a reference straight channel with the same cross-sectional shape. $A(x)$ is the channel cross-section at each axial location.

3. MODEL DEVELOPMENT

The proposed model is based on the analytical solution of the elliptical channel, not because it is likely to occur in practice, but rather to utilize the unique geometrical property of its pressure and velocity solutions. For an elliptical cross-section in the dimensionless Cartesian co-ordinate, pressure gradient up to the first order can be obtained from the equations of motion (i.e. Eqs. (2)-(4)) as follows [30]

$$\left(-\frac{dp}{dx}\right) = \underbrace{\frac{4\pi^2(a^2 + b^2)}{A^3}}_{\text{frictional effect}} - \underbrace{2\varepsilon Re \left(\frac{A'}{A^3}\right)}_{\text{inertia effect}} \quad (8)$$

where $A(x)$ is the local cross-sectional area, $a(x)$ and $b(x)$ are the major and minor axes of the elliptical cross-section along the x -direction, respectively. The prime denotes the rate of change along the flow direction, e.g. $A' = dA/dx$. Channel aspect ratio at each axial location is defined as the ratio of the minor to major axes, i.e. $\gamma(x) = b(x)/a(x)$, which can vary between 0 to 1.

3.1 LUBRICATION APPROXIMATION, $\varepsilon Re \ll 1$

In Eq. (8) the momentum term, i.e. second term, can be neglected if $\varepsilon Re \ll 1$. This yields the "lubrication approximation" [43]. The first term in Eq. (8) resembles the fully developed laminar flow in a straight microchannel of elliptical cross-section and accounts for the frictional effect on the pressure drop. For laminar fully-developed flow in a straight microchannel, it can be shown [44,45] that selection of the channel square root of cross-sectional area, \sqrt{A} , rather than the hydraulic diameter, D_h , leads to similar trends in Poiseuille number for microchannels with a wide variety of cross sections. Therefore, in this study, the square root of a reference straight

microchannel cross-sectional area, $\mathcal{L} = \sqrt{A_0}$, is selected consistently as the length scale throughout the analysis. Using the model of Bahrami et al. [45] at each axial location, frictional pressure gradient, $(-dp/dx)_f$, can be written as follows

$$\left(-\frac{dp}{dx}\right)_f = 16\pi^2\mu Q \frac{I_p^*}{A^2} \quad (9)$$

where Q is the flow rate, $\hat{A}(x)$ is the dimensional cross-sectional area, $I_p^*(x) = I_p/\hat{A}^2$ is the specific polar momentum of inertia [45], and $I_p(x) = \int_{A(x)}(y^2 + z^2)dA$ is the polar momentum of cross-sectional area about its center of geometry. The proposed model postulates that for constant fluid properties and flow rate, the frictional pressure gradient in a slowly-varying cross-section microchannel is only a function of general cross-sectional parameters, i.e. $I_p^*(x)$ and $A(x)$. It can be shown that for channels with similar cross-sectional area and polar moment of inertia, the pressure gradient obtained from Eq. (9) is a weak function of cross-sectional geometrical details, i.e. corners.

3.2 INERTIA EFFECTS, $\varepsilon Re \sim O(1)$

For moderate Reynolds numbers or when εRe becomes in the order of $O(1)$, the second term in Eq. (8) becomes significant and affects the total pressure drop. This term corresponds to the effect of the fluid momentum change along the channel and directly depends on the variation of cross-sectional area (i.e. A'). For a constricted microchannel (i.e. nozzles $A' < 0$), the pressure gradient increases with the Reynolds number and ε but for an expansion microchannel, (i.e. diffusers $A' > 0$), pressure gradient decreases with the Reynolds number and ε . It can be shown that the pressure loss due to the variation of cross-sectional area, $\Delta\hat{p}_{iner}$, is only a function of channel inlet and outlet area and does not depend on the wall shape

$$\Delta\hat{p}_{iner} = \mu\lambda\varepsilon Re \left(\frac{1}{\hat{A}_o^2} - \frac{1}{\hat{A}_i^2}\right) \quad (10)$$

where \hat{A}_i and \hat{A}_o are the channel inlet and outlet cross-sectional area, respectively. Equation (10) clearly shows that for $\hat{A}_i > \hat{A}_o$, the value of $\Delta\hat{p}_{iner}$ is positive and the inertia effect acts in favor of the frictional loss. In contrast, for $\hat{A}_i < \hat{A}_o$, the value of $\Delta\hat{p}_{iner}$ is negative and inertia effect acts against the frictional loss. For $\hat{A}_i = \hat{A}_o$, which occurs in stramwised periodic geometries, such as sinusoidal walls, the inertia effect is zero.

It is beneficial to compare the variation in the pressure loss in a slowly-varying cross-sectional microchannel with that of a reference straight channel with the same cross-sectional shape. This comparison shows the amount of increase in the pressure drop as a result of the deviation from a straight channel.

Defining flow resistance, $R_f = \Delta\hat{p}/Q$, with electrical analogy in mind, one can compute the dimensionless flow resistance $R_f^* = R_f/R_{f,0}$ as follows

$$R_f^* = \int_{x_1}^{x_2} \left[\frac{I_p^*(x)}{I_{p,0}^*} \right] \frac{dx}{A(x)^2} + \frac{\varepsilon Re}{16\pi^2 I_{p,0}^*} \left(\frac{1}{A_0^2} - \frac{1}{A_i^2} \right) \quad (11)$$

where $R_{f,0} = 16\pi^2 \mu \lambda I_{p,0}^* / A_0^2$ is the flow resistance of the reference straight channel with the cross-sectional area of A_0 and the specific polar momentum of inertia of $I_{p,0}^*$. Note that, Eq. (11) can be employed for the calculation of pressure drop in any cross-sectional shape including circle, rectangle, trapezoid, polygon, square, and triangle. Employing Eq. (10), pressure resistance of a microchannel with slowly-varying cross-sectional area can be obtained only by computing the general geometrical parameters and the Reynolds number. On the other hand, using the conventional perturbation technique, velocity distribution must be determined in order to calculate the flow resistance of a channel. For most cross-sections, a closed form of the leading axial velocity terms (i.e. u_0, u_1, \dots) is not available and calculating one may not be possible. This clearly shows the convenience of the proposed general approximate model in Eq. (11). In the following section, compact models are developed for elliptical and rectangular cross-sections and models are compared with available data in the literature and the experimental results of present work.

4. COMPACT MODELS

The general approximate technique introduced in the previous section is implemented and compact relationships are reported for: i) dimensionless flow resistance of elliptical cross-sections with constant aspect ratio, $\gamma(x) = \text{const.} = \gamma_0$ and ii) planar channels with rectangular cross-section (constant height) for three typical wall shapes of linear, sinusoidal and hyperbolic in Table 1. Definitions of the wall profile functions are listed in Table 2. We studied elliptical cross-sections, since they are usually considered in modeling transport processes in porous media [40], furrowed membranes, artificial lung [47], and arterial prostheses [48]. In the case of flow through porous media, since the total pore can be represented by a network of tubes [49], the concept of flow resistance (or inversely flow conductance) is used to determine the pressure drop and permeability of the porous media [49]. Planar geometries with rectangular cross-section can be found in many microfluidics applications such as micromixers [7], accelerate particle electrophoretic separation [18, 19], pre-concentration and separation temperature gradient focusing technique [28, 29]. The hyperbolic geometry is usually used in polymer processing [30, 31].

For the elliptical cross-section, the aspect ratio, $\gamma_0 = b(x)/a(x)$ is kept constant. Here, $a(x)$ and $b(x)$ are the major and minor axes, respectively. The new parameter, $\xi = \delta/a_0$ is called the ‘‘deviation parameter’’ where δ is the difference

between average and maximum value of the major axis and a_0 is the average of the major axis. Note that, the flow resistance of an axisymmetric geometry (i.e. circular cross-section) can be obtained by letting $\gamma_0 = 1$. For the planar geometry with rectangular cross-section, channel height is kept constant, i.e. $b = \text{const.}$, and the mean aspect ratio is defined as $\gamma_0 = b/a_0$ where a_0 is the average width of the microchannel. Since the inertia term is canceled in periodic geometries, Eq. (11) yields the lubrication solution, Eq. (9), and the dimensionless flow resistance becomes independent of the aspect ratio and the Reynolds number. For both linear and sinusoidal walls, at the limiting case when $\xi \rightarrow 0$, the flow resistance yields the solution of straight channel, thus $R_f^* \rightarrow 1$. Another limiting case is when the deviation parameter, ξ , approaches one. For such condition the flow is blocked and the dimensionless flow resistance increases rapidly and approached to infinity.

5. EXPERIMENTAL SETUP

Chemicals and Materials: Distilled water was used as the testing liquid. SU-8 photoresist (Microchem, Newton, MA) and diacetone-alcohol developer solution (Sigma-Aldrich, St. Louis, MO) were used in the making of the positive relief masters by the procedure outlined below. Polydimethylsiloxane (PDMS) casts were prepared by thoroughly mixing the base and curing agent at a 10:1 ratio as per the manufacturer’s instructions for the Sylgard 184 silicon elastomer kit (Dow Corning, Midland, MI).

Table 1. Geometrical parameters for different channel cross-sections.

| Cross-section geometry | wall shape | compact model, R_f^* |
|--|-------------------|--|
| ellipse (constant aspect ratio) | streamwise linear | $\frac{3 + \xi^2}{3(1 - \xi^2)^3}$ |
| | sinusoidal | $\frac{2 + 3\xi^2}{2(1 - \xi^2)^{7/2}}$ |
| | hyperbolic | $R_{fric}^* + R_{iner}^* [\dagger]$ |
| rectangle (planar) | streamwise linear | $\frac{2\xi\gamma_0^2 + (1 - \xi^2)^2 \ln\left(\frac{1 + \xi}{1 - \xi}\right)}{2\xi(1 - \xi^2)^2(1 + \gamma_0^2)}$ |
| | sinusoidal | $\frac{2(1 - \xi^2)^2 + (2 + \xi^2)\gamma_0^2}{2(1 - \xi^2)^{5/2}(1 + \gamma_0^2)}$ |
| | hyperbolic | $R_{fric}^* + R_{iner}^* [\dagger\dagger]$ |
| [\dagger] $R_{fric}^* = \frac{(1 + \beta + \beta^2 + \beta^3 + \beta^4)(\ln\beta)^4}{5(\beta - 1)^4}$ and $R_{iner}^* = \frac{3Re\varepsilon(\beta + 1)\gamma_0(\ln\beta)^4}{4\pi^2(\beta - 1)^3(1 + \gamma_0^2)}$ | | |
| [$\dagger\dagger$] $R_{fric}^* = \frac{[2(\beta - 1)^2 + (\beta^2 + 1)(\gamma_0 \ln\beta)^2](\beta + 1)\ln\beta}{4(\beta - 1)^2(1 + \gamma_0^2)}$ and $R_{iner}^* = \frac{3Re\varepsilon(\beta + 1)\gamma_0(\ln\beta)^2}{4\pi^2(\beta - 1)(1 + \gamma_0^2)}$ | | |

Table 2. Definition of different wall functions.

| wall shape | function |
|--|--|
| | $a(x) = a_0 - 4\delta \left(x + \frac{1}{4}\right); \quad -\frac{1}{2} < x < 0$ $a(x) = a_0 + 4\delta \left(x - \frac{1}{4}\right); \quad 0 < x < \frac{1}{2}$ |
| | $a(x) = a_0 - \delta \cos(2\pi x); \quad -\frac{1}{2} < x < \frac{1}{2}$ |
| | $a(x) = \frac{a_u}{1 + (\beta - 1)x}$ |
| $\beta = \frac{a_u}{a_c}, \quad a_0 = \int_{-1/2}^{1/2} a(x) dx$ | |

Microfabrication: The PDMS/PDMS straight and converging-diverging microchannels were manufactured using the soft lithography technique [50] described in our previous work [51]. Slowly varying cross-sectional microchannel samples were fabricated and tested for the range of $\xi = \delta/a_0 = 0.09 - 0.53$ and $\varepsilon = \sqrt{A_0}/\lambda < 0.1$. Each microchannel contained ten converging-diverging modules with linearly varying wall. Figure 2 shows a labeled photograph of one of the converging-diverging microchannels on a PDMS, $\xi = 0.42$ and $\gamma_0 = 0.32$. The insert is a magnified view of the converging-diverging section under a microscope. Dimensions of the channel were measured by an image processing method; an inverted microscope (Unitron, Commack, NY) equipped with 5X, 0.12 N.A. and 10X, 0.4 N.A. objectives and a CCD camera was used. The low magnification objective was used to measure the length of each module. Images of the channels were taken at three different random locations and then imported in an image processing software (Scopephoto 3.0) in which each pixel was calibrated with an optical ruler (Edmund optics, Barrington, NJ) to measure in-plane geometrical parameters. For each microchannel average values are reported. Through changing the microscope focus, it has been observed that although the channels have somewhat trapezoidal cross-sections, they still can be considered as rectangular with acceptable accuracy. Using the image processing technique described above, the roughness of the channels was estimated

to be less than the accuracy of the image processing method. Thus the roughness effect is neglected in the present study.

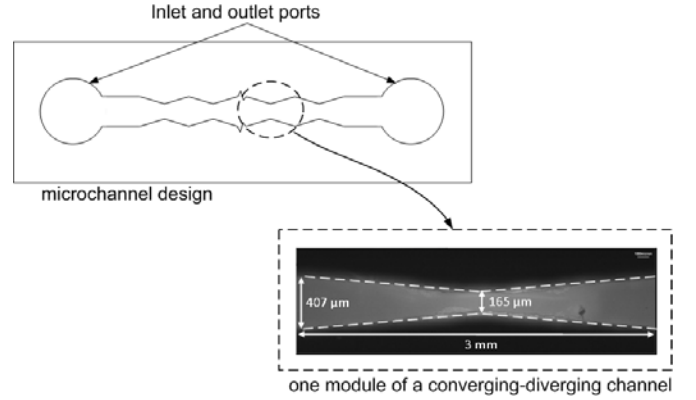


Figure 2. Photograph of a typical converging-diverging microchannel ($\xi = 0.4$) fabricated on a PDMS/PDMS assembly. The inset is a magnified view of one module of converging-diverging section under the microscope. The channel was filled with Rhodamine B for a clear demonstration.

Depth measurement: It has been demonstrated that the conventional theory for flow and pressure drop theory can be used in the micro scale [51-57]. Thus, exact solution for the pressure drop within a straight microchannel of rectangular cross-section was used to determine the microchannel depth. In the absence of the viscous dissipation, streaming potential effects, the bulging of the flexible PDMS material, and the flow resistance for fully developed flow in a microchannel with rectangular cross-section can be obtained accurately from the following relationship [51]

$$\Delta p = \frac{3\mu\lambda Q}{4\hat{b}\hat{a}^3} \left[1 - \frac{192\hat{a}}{\pi^5\hat{b}} \sum_{n=1,3,5,\dots}^{\infty} \frac{\tanh\left(\frac{n\pi\hat{b}}{2\hat{a}}\right)}{n^5} \right]^{-1} \quad (12)$$

where \hat{a} and \hat{b} are the semi-major and semi-minor axes of the cross-section, respectively. Note that the series solution of Eq. (12) converges rapidly. A quick calculation shows that using only the first term of the series predicts the pressure drop within the 99% of the exact solution for the range of $0 \leq \gamma = \hat{b}/\hat{a} \leq 1$. Using Eq. (12) and measuring the pressure drop for a range of flow rate, 30 $\mu\text{L}/\text{min} - 100 \mu\text{L}/\text{min}$ (the corresponding Reynolds number is in the range of 2-15) depth of the converging-diverging channels was determined. In order to ensure that the final straight channel has the same depth as the corresponding converging-diverging channels, both straight and converging-diverging patterns were placed on the same master with the distance of 5 mm from each other. Table 3 summarizes the geometrical parameters of the present experimental work.

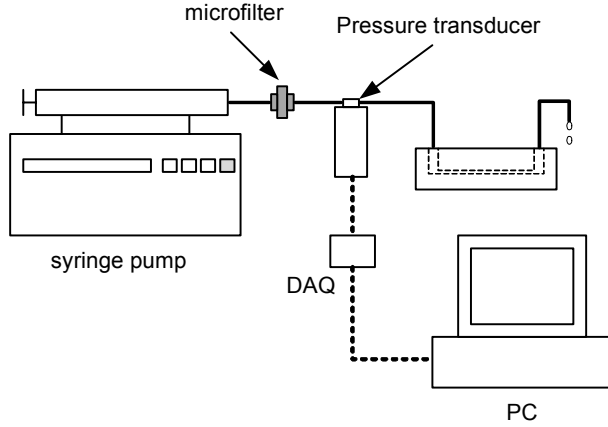


Figure 3. Schematic of the test section.

Pressure measurement: An open loop constant flow rate system, shown in Figure 3, was used for this work. A syringe pump (Harvard Apparatus, QC, Canada) provided constant flow rates with $\pm 0.5\%$ accuracy. A range of Reynolds numbers from 2 – 15 was covered by changing the volumetric flow rate from $30\mu\text{L}/\text{min}$ – $100\mu\text{L}/\text{min}$. Distilled water was forced to flow through a 0.2 micron filter (Aktreingeselchaf Co., Germany) before entering the channel. To measure the pressure drop, a gauge pressure transducer (Omega Inc., Laval, QC, Canada) with the accuracy of $\pm 27\text{ pa}$ ($\pm 0.004\text{ psi}$) was installed at the channel inlet while the channel outlet was opened to the atmosphere. Measured pressure was then monitored and recorded with a data acquisition system (LABVIEW 8.5, National Instruments, USA). The flow was considered to have reached a steady state condition when the readings of the pressure drop did not change with time. For a given channel, the measurement of pressure drop was repeated three times for each flow rate to ensure the reproducibility of the results. An arithmetic averaging method [52] was performed to determine the final results. Maximum difference between the averaged and the actual values was observed to be less than 1.5%. Because of the low Reynolds number, pressure drop due to developing length and minor losses can effectively be neglected [51]. It is also assumed that the viscous heating and channel bulging effects are negligible (see Ref. [51]).

Table 3. Experimental parameters in present work.

| Parameter | Value |
|--------------------|--|
| \hat{a}_{max} | $360\ \mu\text{m} - 433\ \mu\text{m}$ |
| \hat{a}_{min} | $133\ \mu\text{m} - 352\ \mu\text{m}$ |
| \hat{b} | $36\ \mu\text{m} - 94\ \mu\text{m}$ |
| $\sqrt{\hat{A}_0}$ | $118\ \mu\text{m} - 163\ \mu\text{m}$ |
| $\hat{\lambda}$ | 3mm |
| γ_0 | $0.092 - 0.25$ |
| Q | $30\mu\text{L}/\text{min} - 100\mu\text{L}/\text{min}$ |
| Δp | $0.85\text{ kpa} - 24.13\text{ kpa}$ |

6. RESULTS AND DISCUSSION

6.1 MODEL VERIFICATION

As we are primarily interested in the estimation of the of the pressure drop in channels, present study places emphasis on the flow resistance than on the detailed structure of the flow itself. Comparison between the experimental data collected in present work and the analytical models for converging-diverging microchannels with linearly varying cross-section are presented in Figures 4 and 5. As expected, since the geometry of the channels is periodic, inertia effects due to acceleration and deceleration of the flow are cancelling each other and the flow resistance becomes independent of the Reynolds number (see Figure 4). Therefore, for each sample the average value of the dimensionless flow resistance, R_f^* , is taken over the range of Reynolds number and plotted against the values of predicted from Eq. (28) in Figure 7. Good agreement between experimental and analytical compact model can be observed with the difference of less than $\pm 5\%$.

We now compare the results given by present analysis to experimental and numerical data obtained by Oliveira et al. [31] for total pressure drop across a microfluidic rheometric device with application in polymer processing. They [31] measured the pressure drop along a hyperbolic contraction device of rectangular cross-section to evaluate the resistance to the rate of elongation. The geometrical parameters and the flow condition used in their experiment are summarized in Table 4. The improvement offered by the inertia term is obvious in Figure 6, as considering only frictional term substantially underestimates the pressure drop. It can be seen that, most of the data points fall within $\pm 5\%$ of the compact model proposed in Table 1. Due to the sudden expansion of the flow attentively designed by Oliveira et al. [31] to reduce the overall pressure drop, both numerical and experimental data slightly fall below the compact model at higher Reynolds numbers. The linear variation of the dimensionless flow resistance with the Reynolds number in the experimental and numerical data supports our analytical model, Eq. (11), in which for constant geometrical parameters, R_f^* is proportional to the Reynolds number.

6.2. PARAMETRIC STUDY

A parametric study is performed to investigate the effects of relevant geometrical parameters such as aspect ratio and deviation parameter on the pressure field along a sinusoidal channel as an example. Inertia effect on the dimensionless pressure gradient along a sinusoidal tube of elliptical cross-section is investigated for a range of Reynolds number of $Re = 0 - 100$. Variation of dimensionless pressure gradient along a sinusoidal capillary of elliptical cross-section is shown in Figure 7 for three typical deviation parameters of $\xi = 0.1, 0.3,$ and 0.5 and two Reynolds numbers of 0.1 and 100 . The aspect ratio $\gamma_0 = b(x)/a(x)$ and $\varepsilon = \sqrt{\hat{A}_0}/\lambda$ are considered to remain constant along the flow direction holding

typical values of $\gamma_0 = 0.5$ and $\varepsilon = 0.1$, respectively. The pressure gradient in Figure 7 suggests that most of the pressure loss occurs within the throat region. The peak in the pressure gradient occurs at the throat $x = 0$ for low Reynolds number ($Re = 0.1$) while by increasing the Reynolds number ($Re = 100$), the effect of inertia becomes more significant yielding negative pressure gradient and the shift of the peak in the pressure gradient to the converging section. The negative pressure gradient in the throat region of the diverging section for the high Reynolds number ($Re = 100$) confirms the existence of reverse flow. Our analysis shows that there is no evidence of flow reversal for Reynolds numbers lower than 10. The pressure gradient distribution shown in Figure 7 also suggests that for large deviation parameters, reverse flow occurs at lower Reynolds numbers

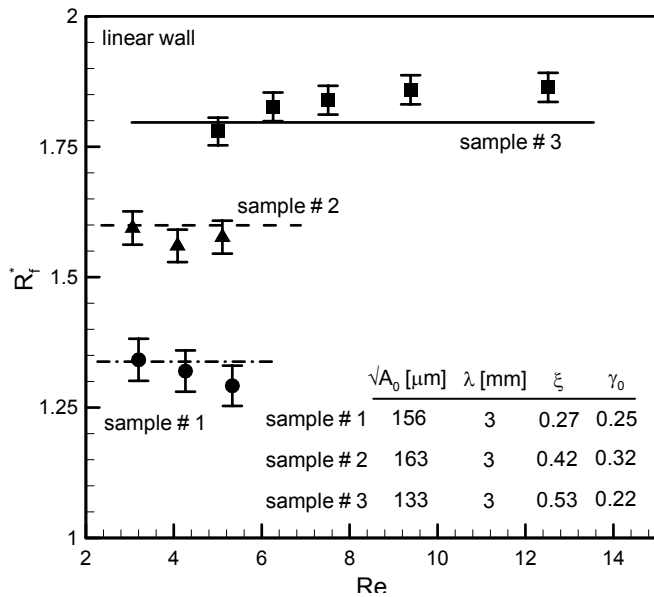


Figure 4. Dimensionless flow resistance as a function of Reynolds number for three different converging-diverging microchannels with linearly varying cross-section. Perturbation parameter, $\varepsilon = \sqrt{A_0}/\lambda$, was always maintained to be less than 0.1. Lines correspond to the analytical model given in Table 2. Circular symbol (\bullet), delta symbol (Δ), and square symbol (\blacksquare) show the experimental results for three different samples of sample #1, sample #2, and sample #3, respectively.

Figure 8 shows the effect of aspect ratio on the dimensionless pressure gradient along the flow direction for an elliptical cross-section. Sinusoidal wall is considered while the deviation parameter and Reynolds number were kept constant (typical values of $\xi = 0.3$ and $Re = 100$). The value of the aspect ratio varies from 0.2 to 1. Pressure gradient is observed to be generally higher for smaller aspect ratios and becomes independent of aspect ratio when $\gamma_0 \rightarrow 1$. The results shown in Figure 8, suggest that flow reversal (which can be used for heat or mass transfer augmentation in micro heat exchangers or micromixers) can be generated by increasing the aspect ratio.

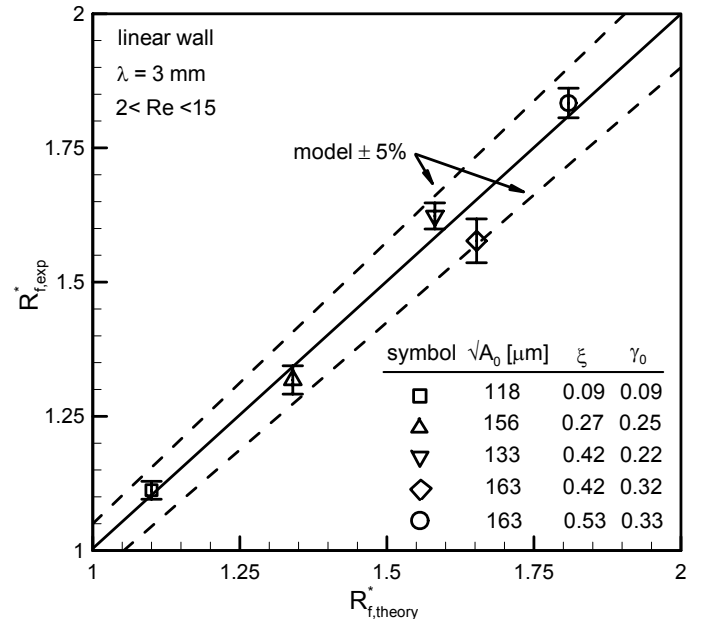


Figure 5. Comparison between experimental data and compact analytical model of Eq. (28) for different converging-diverging microchannels of linearly varying cross-section. Perturbation parameter, $\varepsilon = \sqrt{A_0}/\lambda$, was always maintained to be less than 0.1. Each data point corresponds to the average value of the dimensionless flow resistance over the Reynolds number range of 2-15 for each microchannel.

An independent experimental investigation is also designed and performed for planar periodic microchannels of rectangular cross-section with linear wall profile. The models successfully predict the pressure drop for the collected data within $\pm 5\%$ relative difference range. The experimental data shows that for a periodic geometry, in which the inlet and outlet cross-sectional areas are equal, the inertia effects can reasonably be neglected, as predicted by present analysis. However, for a non-equal inlet and outlet cross-sectional area, considering the frictional effect underestimates the numerical and experimental data.

Our parametric study for a typical sinusoidal wall shows that most of the pressure loss occurs within the throat region. For very low Reynolds number, maximum pressure gradient occurs exactly at the throat while increasing the Reynolds number leads to the flow reversal in the expansion section and shifting the peak in the pressure gradient to the contraction section. Results also show that the deviation parameter has significant effect on the magnitude of the pressure gradient and occurrence of the flow reversal. For larger values of the deviation parameter, the flow reversal occurs at lower Reynolds numbers. Pressure gradient is observed to be generally higher for smaller aspect ratios and becomes independent of aspect ratio when the channel cross-section approaches to the circular cross-section.

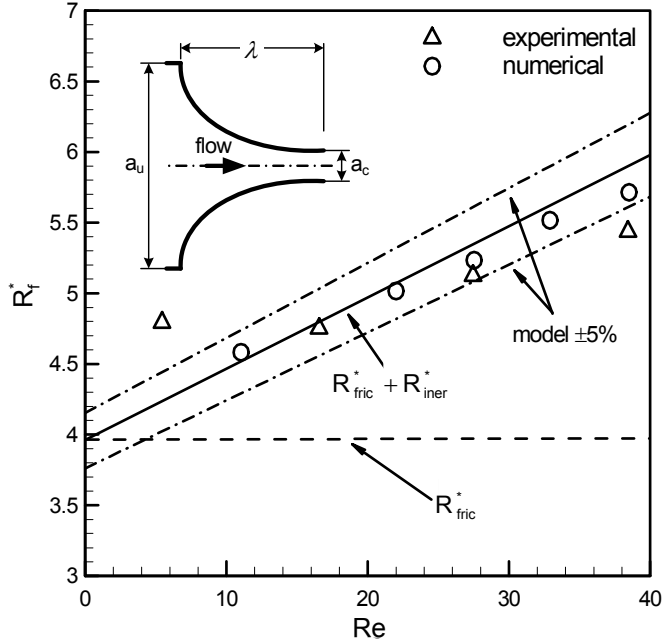


Figure 6. Comparison of theoretical models to experimental and numerical results from Oliviera et al. [31]. The solid line corresponds to the prediction given in Table 2 and the dashed line correspond to the prediction given by the lubrication approximation, i.e. R_{fric}^* . The delta (Δ) and circular (\circ) symbols correspond to the experimental and numerical data from Oliviera et al. [31], respectively with $\beta = \hat{a}_u/\hat{a}_c = 20$, $\gamma_0 = \hat{b}/\hat{a}_0 = 0.73$, $\hat{a}_u = 400 \mu\text{m}$, and $\hat{\lambda} = 382 \mu\text{m}$. The value of the perturbation parameter is $\varepsilon = \sqrt{\hat{A}_0}/\hat{\lambda} = 0.14$.

Table 4. Geometrical and flow conditions used by Oliviera et al. [31].

| Parameter | Value |
|--------------------|--|
| \hat{a}_u | $400 \mu\text{m}$ |
| \hat{a}_c | $19.9 \mu\text{m}$ |
| \hat{b} | $46 \mu\text{m}$ |
| $\sqrt{\hat{A}_0}$ | $54 \mu\text{m}$ |
| $\hat{\lambda}$ | $238 \mu\text{m}$ |
| γ_0 | 0.73 |
| Q | $0.4 \text{ ml/hr} - 10 \text{ ml/hr}$ |
| Δp | $2.18 \text{ kpa} - 16.97 \text{ kpa}$ |

7. SUMMARY AND CONCLUSION

The pressure drop of single phase flow in slowly-varying channels of arbitrary cross-section is investigated in this study. Using the square root of cross-sectional area, $\sqrt{\hat{A}}$, which is shown to be superior to the conventional hydraulic diameter [44, 45], and the asymptotic series solution for the flow through a slowly-varying tube of elliptical cross-section [34], a general model for the prediction of pressure drop within a slowly-varying channel of arbitrary cross-section is proposed. Present analysis shows that the inertia effect on the pressure drop can

be neglected when $\varepsilon \text{Re} \ll 1$ or for streamwised geometries. Compact relationships are proposed for common channel geometries including (i) tubes of elliptical cross-section with constant aspect ratio and (ii) planar channels with rectangular cross-section. As examples, three typical wall shapes of linear, sinusoidal, and hyperbolic are studied in this work. The relationships are compared with the numerical and experimental data collected from the literature.

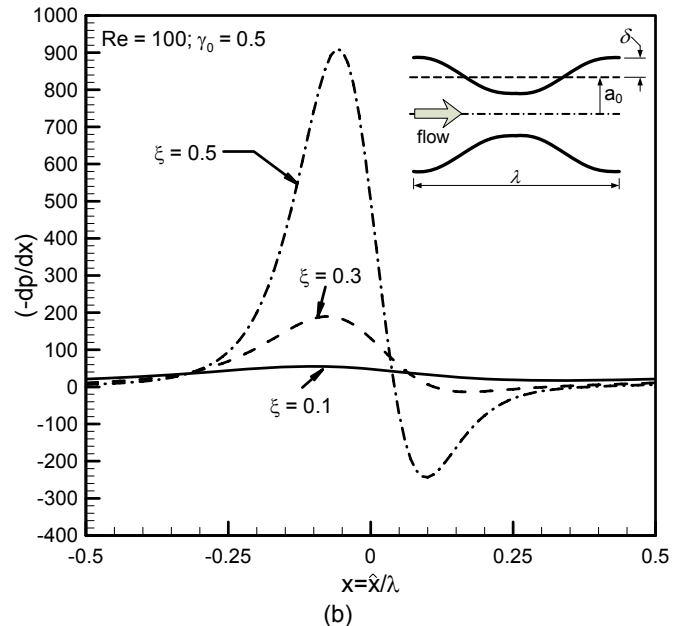
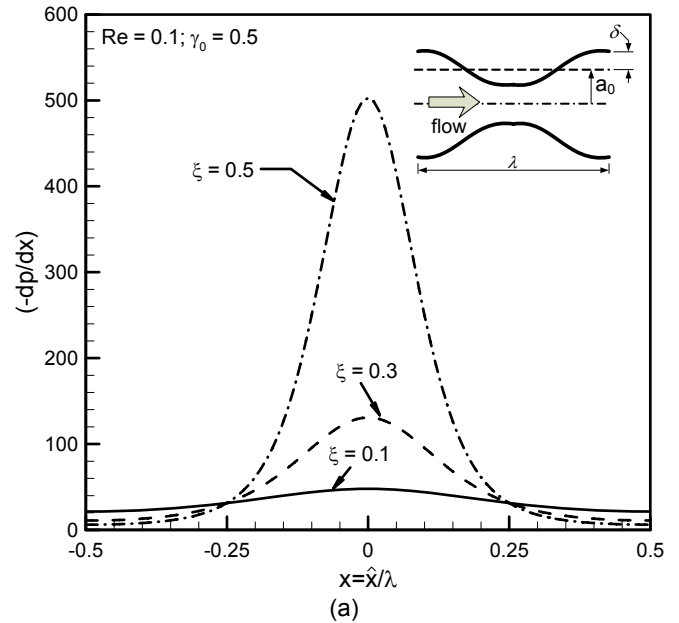


Figure 7. Inertia effect on the pressure gradient along the flow direction for typical values of $\varepsilon = \sqrt{\hat{A}_0}/\hat{\lambda}$ and $\gamma_0 = 0.5$ and (a) $Re = 0.1$ and (b) $Re = 100$. The vertical axis is the dimensionless pressure gradient which can be converted into dimensional pressure gradient through Eq. (6).

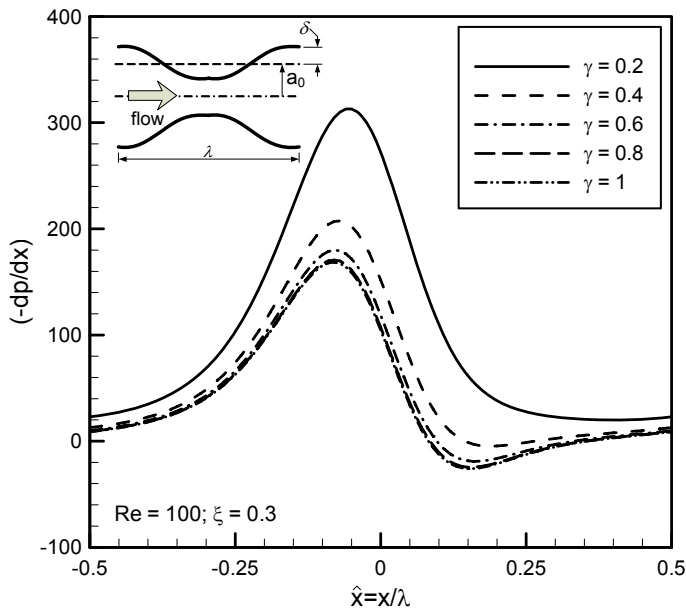


Figure 8. Effect of the aspect ratio on the pressure gradient along the flow direction for a typical deviation parameter of $\xi = 0.3$ and when inertia plays an important role ($Re = 100$).

ACKNOWLEDGMENTS

The authors gratefully acknowledge the financial support of the Natural Sciences and Engineering Research Council of Canada, NSERC. Authors also would like to thank K. Wong for his kind help during the experimental measurements.

REFERENCES

- [1] Burns, M.A., Johnson, B.N., Brahmamandra, S.N., Handique, K., Webster, J.R., Krishnan, M., Sammarco, T.S., Man, P.M., Jones, D., Heldsinger, D., Mastrangelo, C.H., and Burke D.T., An Integrated Nanoliter DNA Analysis Device, *Science* 282 (1998) 484-487.
- [2] Chou, H.P., Spence, C., Scherer, A., and Quake, S. R. A microfabricated device for sizing and sorting DNA molecules, *Proc. Natl. Acad. Sci. U.S.A.* 96 (1999) 11-13.
- [3] Sakaki, K., Foulds, I.G., Liu, W., Dechev, N., Burke, R.D., and Park, E.J., RoboSCell: an automated single cell arraying and analysis instrument, *Biomedical Microdevices* 11(6) (2009) 1317-1330.
- [4] Dunn, D. A. and Feygin, I., Challenges and solutions to ultra-high-throughput screening assay miniaturization: Submicroliter fluid handling, *Drug Discovery Today* 5 (2000) S84-S91.
- [5] Losey, M. W., Schmidt, M. A., and Jensen, K. F., Microfabricated Multiphase Packed-Bed Reactors: Characterization of Mass Transfer and Reactions, *Ind. Eng. Chem. Res.* 40, (2001) 2555-2562.
- [6] Sammarco, T. S. and Burns, M. A., Thermocapillary pumping of discrete drops in microfabricated analysis devices, *AICHE J.* 45 (1999) 350-366.
- [7] Lauga, E., Strook, A., and Stone, H.A., Three-dimensional flows in slowly varying planar geometries, *Physics of Fluids* 16(8) (2004) 3051-3062.
- [8] Strook D.A., Stroock, A.D., Dertinger, S.K.W., Ajdari, A., Howard, I.M., Stone, A., Whitesides, G.M., "Chaotic mixers for microchannels", *Science* 295 (2002) 647-651.
- [9] Hsieh, S.S. and Huang, Y.C., Passive mixing in microchannels with geometric variations through μ PIV and μ LIF measurements, *J. Micromech. Microeng.* 18, (2008) 065017.
- [10] Bessoth, F.G., deMello, A.J., and Manz, A., Microstructure for efficient continuous flow mixing, *Anal. Commun.* 36 (1999) 213-215.
- [11] Liu, R.H., Sharp, K.V., Olsen, M.G., Stremler, M.A., Santiago, J.G., Adrian, R.J., Aref, H., and Beebe, D.J. A passive three-dimensional 'C-shape' helical micromixer, *J. Microelectromech. Syst.* 9 (2000) 190-197.
- [12] Bertsch, A., Heimgartner, A., Cousseau, P., and Renaud, P., Static micromixers based on large-scale industrial mixer geometry, *Lab Chip* 1 (2001) 56-60.
- [13] Johnson, T.J., Ross, D., and Locascio, L.E., Rapid microfluidic mixing, *Anal. Chem.* 74 (2002) 45-51.
- [14] Rife, J.C., Bell, M.I., Horwitz, J.S., Kabler, M.N., Auyeung, R.C.Y., and Kim, W.J., Miniature valveless ultrasonic pumps and mixers, *Sens. Actuators A* 86, (2000) 135-140.
- [15] Lee, Y.K., Deval, J., Tabeling, P., and Ho, C.M., Chaotic mixing in electrokinetically and pressure driven micro flows, *Micro Electro Mechanical Systems, 2001. MEMS 2001. The 14th IEEE International Conference*, (2001) 483-486.
- [16] Knight, J.B, Vishwanath, A., Brody, J.P, and Austin, R.H., Hydrodynamic focusing on a silicon chip: mixing nanoliters in microseconds, *Phys Rev Lett.* 80 (1998) 3863-3866.
- [17] Veenstra, T.T., Lammerink, T.S.J., Elwenspoek, M.C., Van Den Berg, A., Characterization method for a new diffusion mixer applicable in micro flow injection analysis systems, *J Micromech. Microeng.* 9 (1998) 199-202.
- [18] Xuan, X., Xu, B., and Li. D., Accelerated particle electrophoretic motion and separation in converging-diverging microchannels, *Anal. Chem.* 77 (2005) 4323-4328.
- [19] Xuan, X., and Li. D., Particle motions in low-Reynolds number pressure-driven flows through converging-diverging microchannels, *J. Micromech. Microeng.* 16 (2006) 62-69.
- [20] Sparrow, E. M. and A. T. Prata, Numerical solutions for laminar flow and heat transfer in a periodically converging-diverging tube, with experimental confirmation, *Numerical Heat Transfer* 6 (1983) 441-461.
- [21] Wang, G. and Vanka, S. P., Convective heat transfer in periodic wavy passages, *Int. J. of Heat and Mass Transfer* 38 (17) (2000) 3219-3230.
- [22] Nishimura, T., Bian, Y. N., Matsumoto, Y., and Kunitsugu, K., Fluid flow and mass transfer characteristics in a sinusoidal wavy-walled tube at moderate Reynolds numbers for steady flow, *Journal of Heat and Mass Transfer* 39 (2003) 239-248.
- [23] Lahbabi, A. and Chang, H. C., Flow in periodically constricted tubes: transition to inertial and nonsteady flows, *Chem. Eng. Sci.* 41 (1986) 2487-2505.

- [24] Payatakes, A. C., Tien, C., and Turian, R. M., A new model for granular porous media: Parts 1 and 2, *AIChE J.* 19(1) (1973) 58-67.
- [25] Bernabe Y. and Olson, J. F., The hydraulic conductance of a capillary with a sinusoidally varying cross-section, *Geophys. Res. Lett.* 27 (2000) 245-248.
- [26] Tamayol, A. and Bahrami, M. Analytical determination of viscous permeability of fibrous porous media, *Int. J. of Heat and Mass Transfer* 52 (2009) 2407–2414.
- [27] J. H. Forrester and D. F. Young, Flow through a converging–diverging tube and its implications in occlusive vascular disease, *J. Biomech.* 3(3) (1970) 307-310.
- [28] Ross, D. and Locascio, L.E., Microfluidic temperature gradient focusing, *Anal. Chem.* 74 (2002) 2556-2564.
- [29] Kim, S.M., Sommer, G.J., Burns, M.A., Hasselbrink, E.F., Low-power concentration and separation using temperature gradient focusing via joule heating, *Anal. Chem.* 78 (2006) 8028-5035.
- [30] James, D.F., Flow in a converging channel at moderate Reynolds number, *AIChE* 37(1) 59-64.
- [31] Oliviera, M.S.N., Alves, M.A., Pinho, F.T., and McKinley, G.H., Viscous flow through microfabricated hyperbolic contractions, *Experiments in fluids* 43(2-3) 437-451.
- [32] Manton, M.J., Low Reynolds number flow in slowly varying axisymmetric tubes, *J. Fluid Mech.* 49 451-459.
- [33] Van Dyke, M., Slow variations in continuum mechanics, *Adv. Appl. Mech.* 25 (1987) 1-43.
- [34] Wild, R., Pedley, T.J., and Riley, D.S., 1977, “Viscous flow in collapsible tubes of slowly varying elliptical cross-section”, *J. Fluid Mech.* 81, pp. 273-294.
- [35] Payatakes, A. C., Tien, C., and Turian, R. M., A new model for granular porous media: Parts 1 and 2, *AIChE J.* 19(1) (1973) 58-67.
- [36] Sisavath, S., Jing, X., Zimmerman, R.W., Creeping flow through a pipe of varying radius, *Physics of Fluids* 13 (10) (2001) 2762-2772.
- [37] Brod, H., Invariance relations for laminar forced convection in ducts with slowly-varying cross-section, *Int. J. Heat and Mass Transfer* 44 (2001) 977-987.
- [38] Akbari, M., Sinton, D., Bahrami, M., Laminar fully developed flow in periodically converging-diverging microtubes, *Heat Transfer Engineering* 31 (8) 624-634.
- [39] Wang, G. and Vanka, S. P., Convective heat transfer in periodic wavy passages, *Int. J. of Heat and Mass Transfer* 38 (17) (2000) 3219-3230.
- [40] Hemmat, M. and Borhan, A., Creeping flow through sinusoidally constricted capillaries, *Physics of Fluids* 7 (9) (1995) 2111-2121.
- [41] Nishimura, T., Bian, Y. N., Matsumoto, Y., and Kunitsugu, K., Fluid flow and mass transfer characteristics in a sinusoidal wavy-walled tube at moderate Reynolds numbers for steady flow, *Journal of Heat and Mass Transfer* 39 (2003) 239-248.
- [42] Deiber, J.A. and Schowalter, W.R., Flow through tubes with sinusoidal axial variations in diameter, *AIChE* 25 (1979) 638-644.
- [43] Sisavath, S., Al-Yaarubi, A., Pain, C.C., Zimmerman, R.W., A simple model for deviations from cubic law for a fracture undergoing dilation or closure, *Pure appl. geophys.* 160 (2003) 1009-1022.
- [44] Muzychka, Y.S. and Yovanovich, M.M., Laminar flow friction and heat transfer in non-circular ducts and channels part 1: Hydrodynamic problem, *Compact Heat Exchangers, A Festschrift on the 60th Birthday of Ramesh K. Shah, Grenoble, France* (2002) 123-130.
- [45] Bahrami, M., Yovanovich, M. M., and Culham, J. R., A novel solution for pressure drop in singly connected microchannels”, *Int. J. of Heat and Mass Transfer* 50 (2007) 2492-2502.
- [46] Timoshenko, S.P. and Goodier, J.N., *Theory of Elasticity*, (1970) McGraw-Hill Inc., New York, Chapter 10.
- [47] Sobey, I.J., On flow through furrowed channels. Part 1: calculated flow patterns, *J. Fluid Mech.* 96 (1980) 1-26.
- [48] Savvides, G.N. and Gerrard, J.H., Numerical analysis of the flow through a corrugated tube with application to arterial prostheses, *J. Fluid Mech.* 138 (1984) 129-160.
- [49] Koplik, J., Creeping flow in two-dimensional networks, *J. Fluid Mech.* 119 (1982) 219-247.
- [50] McDonald, J.C., Duffy, D.C., Anderson, J.R., Chiu, D.T., and Wu, H., Schueller, G.M. Whiteside, Fabrication of microfluidic systems in poly(dimethylsiloxane), *Electrophoresis* 21 (2000) 27-40.
- [51] Akbari, M., Sinton, D., and Bahrami .M., Pressure drop in rectangular microchannels as compared to theory based on arbitrary cross-section, *ASME J. of Fluids Engineering* 131 (2009) 041202-1-8.
- [52] Jiang, X. N., Zhou, Z. Y., Huang, X. Y., and Liu, C. Y., Laminar Flow Through Microchannels Used for Microscale Cooling Systems,” *IEEE/CPMT Electronic Packaging Technology Conference* (1997) 119–122.
- [53] Judy, J., Maynes, D., and Webb, B. W., Characterization of Frictional Pressure Drop for Liquid Flows Through Microchannels,” *Int. J. Heat Mass Transfer*, 45 (2002) 3477–3489.
- [54] Gao, P., Le Person, S., and Favre-Marinet, M., Scale Effects on Hydrodynamics and Heat Transfer in Two-Dimensional Mini and Microchannels,” *Int. J. Therm. Sci.*, 41 (2002) 1017–1027.
- [55] Wu, H. Y., and Cheng, P., Friction Factors in Smooth Trapezoidal Silicon Microchannels With Different Aspect Ratios, *Int. J. Heat Mass Transfer* 46 (2003) 2519–2525.
- [56] Liu, D., and Garimella, S., “Investigation of liquid flow in microchannels,” *J. Thermophys. Heat Transfer* 18 (2004) 65–72.
- [57] Baviere, R., Ayela, F., Le Person, S., and Favre-Marinet, M., Experimental characterization of water flow through smooth rectangular microchannels, *Phys. Fluids* 17 (2005) 098105.
- [51] White, F. M., *Viscous Fluid Flow*, (1974) McGraw-Hill, New York, Chap. 3.
- [52] Holman, J. P., *Experimental Methods for Engineering*, 7th ed., McGraw-Hill, New York, (2001) Chap.